Temperature Profile Inside Microscale Thermoelectric Module Acquired Using Near-Infrared Thermoreflectance

Rajeev Singh, Joachim Nurnus, Zhixi Bian, James Christofferson, and Ali Shakouri

***Abstract*—We present high-resolution thermal images of the electrical contacts inside an active thermoelectric micromodule that are acquired through the silicon substrate using near-infrared thermoreflectance. The temperature distribution of the contacts induced by the Peltier and Joule effects are separated. This technique can be utilized as a nondestructive means to evaluate metallization and contact resistance of micrometer-scale thermoelectric modules. By determining localized sources of Joule heating, one can identify manufacturing errors and generate design rules that can improve the cooling performance of the thermoelectric device.**

***Index Terms*—Contacts, infrared (NIR) imaging, thermoelectric devices, thermooptic effects, wafer bonding.**

I. Introduction

As THE transistor densities and clock speeds of integrated circuits increase, their high power dissipation densities demand stringent cooling requirements. In particular, the nonuniform power distributions and the large heat flux densities of modern integrated circuits necessitate cost-effective cooling solutions capable of large cooling power densities at high spatial resolutions. Bulk thermoelectric cooling modules cannot effectively target localized regions of heating in integrated circuits due to their large surface areas and relatively low cooling power densities on the order of 1–5 $\mathrm{W \cdot cm^{-2}}$, mainly limited by their long element lengths [1]. Thermoelectric micromodules can efficiently solve these problems by incorporating smaller cold-side areas for localized cooling with shorter leg lengths for greater cooling power densities on the order of 100 $\mathrm{W \cdot cm^{-2}}$. In addition, thermoelectric micromodules have a fast transient response on the order of 10^{-3} seconds and can therefore provide high-frequency cooling for specific applications [2].

A thermoelectric module's coefficient of performance (COP) is a strong function of its element length due to the parasitic effect of contact and metallization resistance. Fig. 1 is a plot of the calculated COP versus element length for a thermoelectric module composed of conventional Bi_2Te_3 material (n- and p-type material properties are assumed identical other than opposite Seebeck coefficient polarity) for cold- and hot-side temperatures of 275 and 300 K, respectively, and for contact resistivities ranging from 10^{-5} $\Omega\mathrm{cm}^2$ to 10^{-8} $\Omega\mathrm{cm}^2$ [3]. The calculation only considers the parasitic effect of finite contact resistivity, and the maximum COP for the case of zero contact resistance is also plotted.

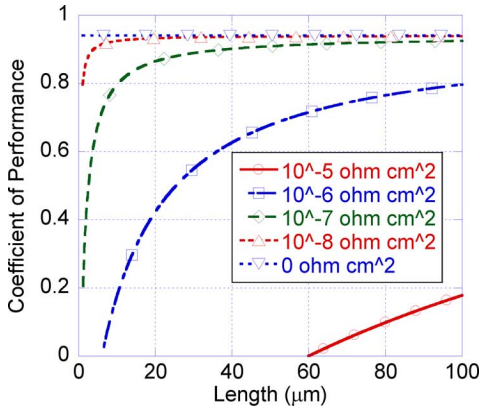

Fig. 1. COP of an n-element Bi_2Te_3-based thermoelectric module as a function of element length for different contact resistivities and for the maximum COP case of zero contact resistance.

We utilize near-infrared (NIR) thermoreflectance through silicon substrate to determine the temperature distribution on the cold-side electrical contacts of an active thermoelectric module whose elements are 20 μm long. Lock-in detection at the first and second harmonics of the device excitation frequency permit the extraction of the temperature distributions due to the Peltier and Joule effects. This technique can be useful for nondestructive characterization of the metallization inside thermoelectric modules by detecting localized regions of excessive ohmic heating and can also be used to determine Peltier cooling uniformity. Since the thermoelectric micromodules are fabricated using a wafer-scale approach, NIR thermoreflectance can be used as a diagnostic tool to improve fabrication processes to maximize the COP of the devices.

II. Thermoelectric Micromodule Fabrication

The fabrication of thermoelectric micromodules is accomplished using a wafer-scale approach to maximize yield and reduce costs [4]. Micrometer-scale thermoelectric modules are

Manuscript received February 13, 2008; revised August 27, 2008. First published March 24, 2009; current version published July 22, 2009. This work was supported in part by grants from National Semiconductor, SRC IFC, and ONR MURI TEC Center. This work was recommended for publication by Associate Editor T. Schoepf upon evaluation of the reviewers comments.

R. Singh, Z. Bian, J. Christofferson, and A. Shakouri are with the Electrical Engineering Department, University of California, Santa Cruz, CA 95064 USA (e-mail: rsingh@soe.ucsc.edu; zxbian@soe.ucsc.edu; jchrist@soe.ucsc.edu; ali@soe.ucsc.edu).

J. Nurnus is with Micropelt GmbH, 79110 Freiburg, Germany (e-mail: joachim.nurnus@micropelt.com).

Color versions of one or more of the figures in this paper are available online at http://ieeexplore.ieee.org.

Digital Object Identifier 10.1109/TCAPT.2008.2011886

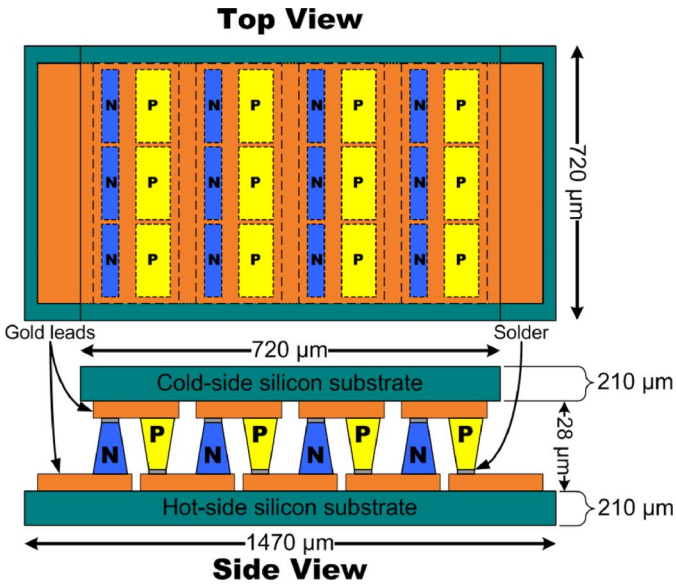

Fig. 2. Schematic of an eight element thermoelectric micromodule in top-view (cutaway) and side view (not to scale). The length of the thermoelectric elements is 20 μm.

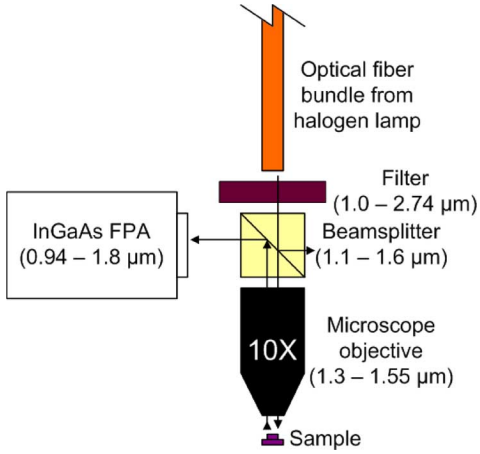

Fig. 3. Diagram of the NIR thermoreflectance experiment showing all optical components and their greater than 50% transmission windows. The indicated FPA window is for a detector responsivity greater than 0.05 A/W.

fabricated by deposition of complementary contacts for many modules onto standard 4-in semi-insulating silicon wafers to form the two sides of the modules (an n-type side and a p-type side). N- and p-type thermoelectric materials based on Bi_2Te_3 are then deposited via sputtering on the contacts of the corresponding wafers. A solder material is then deposited onto the thermoelectric material before the layers are dry-etched to form elements. Next, the wafers are diced to form the halves of many modules. Finally, the n-type half-module and the p-type half-module are joined via soldering. A schematic of an eight-element thermoelectric micromodule designed for size-matched cooling of lasers and sensors is shown in Fig. 2. The length of the thermoelectric elements in the investigated module is 20 μm. Although the module used in the experiments presented here is from an older design generation that is capable of a maximum cooling temperature difference of approximately 39 K at a hot-side temperature of 300 K, current state-of-the-art modules are reported to achieve a maximum cooling temperature difference of over 60 K at 300 K [5].

III. Thermoreflectance Microscopy

Thermoreflectance microscopy is a technique frequently applied to measure surface temperature maps of active semiconductor devices with high spatial and temperature resolutions. Thermoreflectance utilizes the finite temperature dependence of the surface reflectivity of materials to determine the surface temperature. By measuring the change of the illumination intensity reflected from a surface due to a temperature change, the thermal image can be obtained. The first-order approximation of the relationship between the change in surface temperature and the change in surface reflectivity is given as

$$\Delta T = \left(\frac{1}{R}\frac{\partial R}{\partial T}\right)^{-1}\frac{\Delta R}{R} = \kappa^{-1}\frac{\Delta R}{R} \qquad (1)$$

where ΔT is the change in surface temperature in units K, R is the reflected illumination intensity from the surface of the sample, and κ is the thermoreflectance coefficient in units K^{-1} [6]. The value of κ depends on the sample's surface material, the wavelengths of the illumination source, and the experimental conditions such as the numerical aperture of the microscope objective used for magnification [7]. The κ for a particular experimental arrangement can be determined by measuring ΔR for a known ΔT. Although the thermoreflectance technique is reported to achieve a 10-mK temperature resolution and a 250-nm spatial resolution using illumination at 467 nm [8], there is little published work in the application of thermoreflectance at wavelengths in the infrared regime.

IV. NIR Thermoreflectance

Longer wavelength thermoreflectance can be useful due to the ability to image through semiconductor material using illumination wavelengths whose energies are below the bandgap of the material. Many state-of-the-art CMOS integrated circuits are flip-chip bonded to their package leads, prohibiting visible access to the device contacts. In this case, thermoreflectance can be applied at wavelengths whose energies are below the bandgap of the device substrate to image the temperature distribution on the contacts through the backside of the device. An initial report of backside thermoreflectance imaging at wavelengths in the NIR regime using coherent sources of illumination is complicated by Fabry–Perot effects inside the substrate and is limited to scanned point measurements [9]. Subsequent work on NIR thermoreflectance utilizes broadband incoherent illumination and an InGaAs focal-plane array (FPA) imager along with a numerical aperture-increasing lens (NAIL) to solve many problems associated with NIR thermoreflectance [10]. The work presented here utilizes incoherent NIR illumination along with a FPA imager to conduct thermoreflectance experiments on an active thermoelectric micromodule. The simple experimental configuration is shown in Fig. 3 along with the greater than 50% transmission windows of all optical components and the FPA window for detector responsivity greater than 0.05 A/W. A halogen lamp coupled to a fiber optic bundle is used as the illumination source.

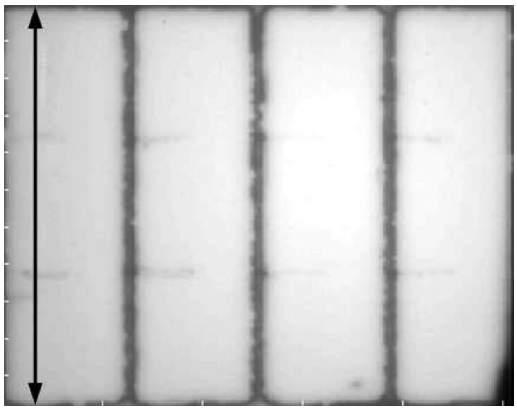

Fig. 4. DC image of the top of the cold-side gold contacts of the mircothermoelectric device acquired through the cold-side silicon substrate. The arrow indicates the position of the cross-sectional line-scan shown in Fig. 6.

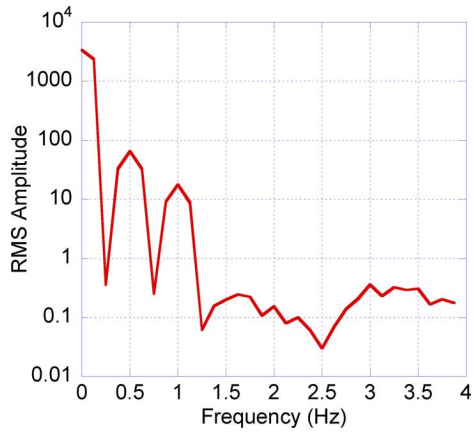

Fig. 5. FFT rms amplitude spectrum of the thermoreflectance signal from a point on the device cold-side gold contact due to a sinusoidal current at 0.5 Hz of 861-mA amplitude with no dc offset. This current amplitude corresponds to Peltier- and Joule-induced ΔTs of 58 and 31 K, respectively. The FPA camera is operated at a frame rate of 8 Hz with a measurement time constant of 8 s.

Subsequent filtration of the halogen source removes the visible components from its spectrum. The thermoelectric sample device is mounted on a xyz translation stage for positioning and focusing. The sample stage is heated to 320 K in order to avoid condensation of water on the thermoelectric device due to the low cold-side temperatures that it can achieve relative to ambient in the cooling mode.

V. Results

Fig. 4 is a dc image of the cold-side gold contacts of the microthermoelectric device acquired through the silicon substrate. The four individual gold contacts are clearly seen in the image. In order to acquire the ac signal resulting from steady-state temperature variations due to the Peltier and Joule effects, the device is activated with an ac current at a frequency of 0.5 Hz at various amplitudes with no dc component. The FPA camera is operated at a frame rate of 8 Hz with an 8-s measurement time constant. Lock-in detection is used to determine the thermoreflectance signal amplitude at the first (Peltier) and second (Joule) harmonics. Fig. 5 is the fast Fourier transform (FFT) spectrum of the thermoreflectance signal from a point on the device's contact metallization. The spectrum contains peaks due

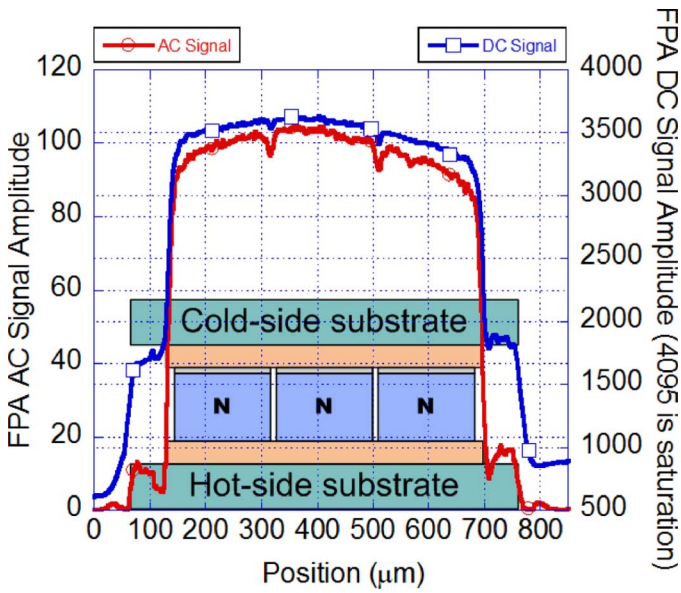

Fig. 6. Cross-section of the dc and ac thermoreflectance signal amplitudes due to the Peltier effect for a sinusoidal current amplitude of 861 mA, corresponding to a ΔT of 58 K. The average noise floor of the FPA is approximately 72.

to Peltier and Joule effect-induced temperature variations. The arrow in Fig. 4 indicates the position of the scan presented in Fig. 6 that shows the dc and ac thermoreflectance signal at the first harmonic acquired across the device. It is clear from Fig. 6 that there is a significant amount of reflection from the silicon. Although dc reflection is subject to variations in surface illumination, the measured dc contrast ratio between a point on the substrate above a gold contact and a point on the substrate outside of the gold contact area is 2.13. Calibration of the effective κ above the buried gold-silicon interface is achieved by modulating the device temperature at 0.5 Hz in order to ensure isothermal conditions between the gold contacts and the top surface of the silicon substrate where a microthermocouple of 13-μm-diameter leads is placed. A value of 4.54×10^{-4} K^{-1} is obtained for the effective κ of the device above the gold contact. Assuming isothermal conditions on the device cold side, the calculated effective κ of the substrate outside of the gold contact area is 1.01×10^{-4} K^{-1}. The average surface temperature of the four gold contacts due to the Peltier and Joule effects versus applied sinusoidal device current is shown in Fig. 7. The measured temperatures are in excellent agreement with the data obtained using a microthermocouple placed on top of the cold-side substrate. The temperature change measured with the microthermocouple due to the Peltier and Joule effects are extracted using dc currents of opposite polarities as follows:

$$\Delta T_{\text{Peltier}} = \left| \frac{\Delta T(+I_{DC}) - \Delta T(-I_{DC})}{2} \right| \tag{2}$$

and

$$\Delta T_{\text{Joule}} = \left| \frac{\Delta T(+I_{DC}) + \Delta T(-I_{DC})}{2} \right|. \tag{3}$$

Figs. 8 and 9 are the resulting thermal images due to the Peltier and Joule effects, respectively, for a sinusoidal device current amplitude of 861 mA at 0.5 Hz. In both images, the FPA camera

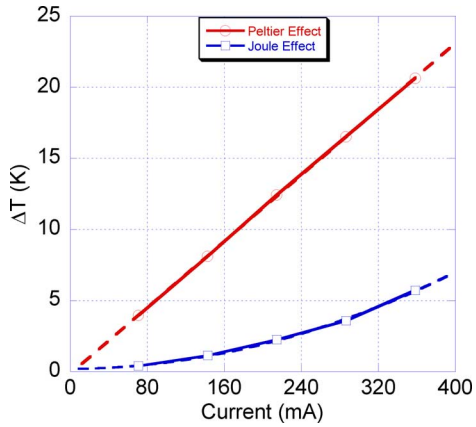

Fig. 7. Measured average thermoreflectance temperature above gold contacts versus applied sinusoidal device current at 0.5 Hz due to the Peltier and Joule effects (solid lines) for an effective $\kappa = 4.54 \times 10^{-4}$ K^{-1}. The ΔT due to the Peltier and Joule effects are fitted (dashed line) to linear and second-order equations, respectively.

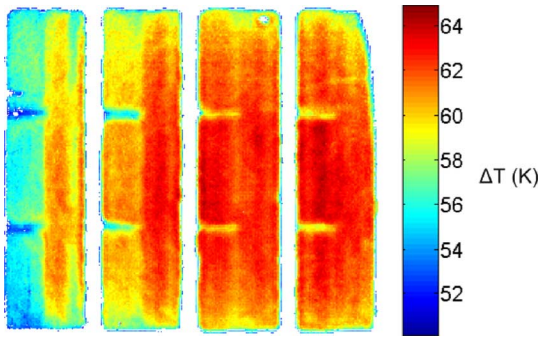

Fig. 8. Thermal image on the top of the gold contacts on the cold-side of the microthermoelectric module due to the Peltier effect for a sinusoidal current amplitude of 861 mA at 0.5 Hz.

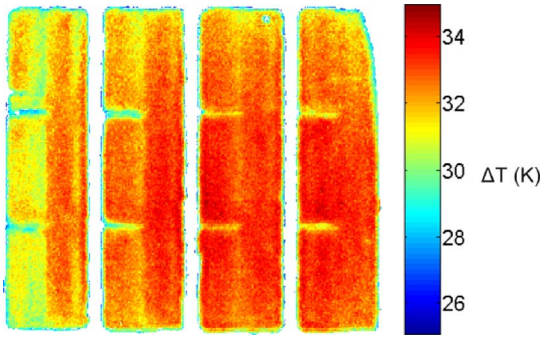

Fig. 9. Thermal image on the top of the gold contacts on the cold-side of the microthermoelectric module due to the Joule effect for a sinusoidal current amplitude of 861 mA at 0.5 Hz.

is operated in full-frame mode for a pixel count of 320×256 which limits the acquisition rate to 20 Hz. The figures reveal a column of defective thermoelectric legs in the left-hand side of the module. For comparison, the FPA camera is windowed to 128×128 pixels to increase the system frame rate to a maximum of 100 Hz. This enables device modulation frequencies to extend as high as approximately 25 Hz while capturing both Peltier and Joule effect-induced temperature distributions. The resulting lower spatial resolution thermal images are shown in

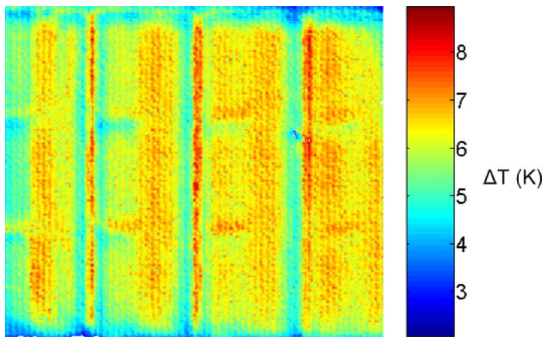

Fig. 10. Thermal image on the top of the gold contacts on the cold-side of the microthermoelectric module due to the Peltier effect for a sinusoidal current amplitude of 861 mA at 22 Hz.

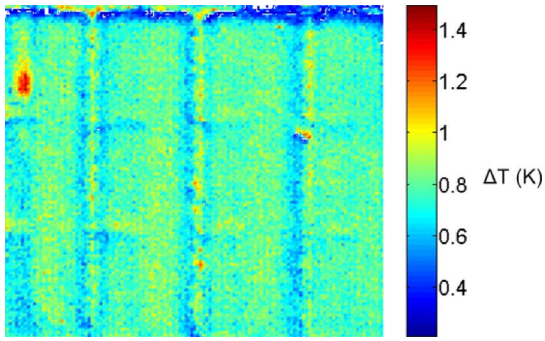

Fig. 11. Thermal image on the top of the gold contacts on the cold-side of the microthermoelectric module due to the Joule effect for a sinusoidal current amplitude of 861 mA at 22 Hz.

Figs. 10 and 11, respectively, for the Peltier and Joule effects for a measurement time constant of 2 s. For identical current amplitudes, the average surface ΔT for device modulation at 22 Hz is substantially less than for device modulation at 0.5 Hz because the device cold-side cannot achieve the maximum ΔT for a given current amplitude at the higher modulation frequency. As the device modulation frequency is increased, the measured ΔT becomes increasingly localized to the source of heat flux. In this regard, we can obtain a more detailed knowledge of the sources of heat flux in the device. Six individual thermoelectric legs within the perimeter of each metal contact can be discerned in the Peltier effect-induced thermal image in Fig. 10. Although the temperature distribution shown in Fig. 11 due to the Joule effect is relatively uniform, a localized source due to parasitic Joule heating is revealed. This suggests that device processing relating to electric contact formation can be improved. In addition, the ratio of the measured ΔT on the cold-side metallization due to the Peltier effect at 0.5 and 22 Hz is 10, while the ratio due to the Joule effect at the same frequencies is 32. Since the Peltier effect occurs at the metal-semiconductor interface (the point of thermoreflectance measurement), the frequency response of the Peltier effect-induced ΔT will be greater than the frequency response of the Joule effect-induced ΔT if the dominant source of Joule heating is not at the metal-semiconductor interface. Therefore, the dominant source of Joule heating in the module must either be in the bulk Bi_2Te_3 material or at the hot-side metal-semiconductor interface.

VI. Conclusion

We have utilized NIR thermoreflectance to image the temperature distribution on top of the cold-side metallization of a microthermoelectric module with 20 μm element length. The images presented are acquired through silicon substrate that is 210 μm thick. Incident illumination is filtered halogen light. The detector is an InGaAs FPA camera that achieves a maximum frame rate of 20 Hz for a 320×256 pixel count and a maximum rate of 100 Hz for a 128×128 pixel count in our acquisition system. An effective κ of 4.54×10^{-4} K^{-1} is measured for signals detected above the gold contact. A calculated value of the effective κ of the cold-side silicon substrate in regions outside of the gold area is 1.01×10^{-4} K^{-1}. By utilizing sinusoidal active device modulation in conjunction with lock-in detection, we successfully extract the temperature distributions on the embedded gold contacts due to the Peltier and Joule effects, even for device modulation frequencies as low as 0.5 Hz.

Because the COP of a thermoelectric device becomes a strong function of contact and interconnect resistance as the element length enters the micrometer regime, an important application of this technique is in the nondestructive evaluation of active micrometer-scale thermoelectric device performance.

Future work will focus on extending the NIR thermoreflectance measurement frequency response beyond what is afforded by the FPA camera thorough the use of heterodyne detection described in detail in [11]. Heterodyne detection at higher frequencies will permit the resolution of extremely localized heat fluxes in the device. An experimental arrangement will be devised to measure the temperature distribution on the hot-side electrical contacts of thermoelectric micromodules while the cold-side of the device is heat sinked. In addition, a high-power LED array emitting at 1.55 μm will be used as the illumination source in order to improve the contrast ratio between metal leads beneath the silicon and the silicon itself. The use of a narrow spectrum source centered at 1.55 μm can result in a more defined measurement of experimental κ at the metal-semiconductor interface. In this case, the use of a NAIL as described in [10] can increase the spatial resolution of the measurement.

References

[1] J. W. Vandersande and J.-P. Fleurial, "Thermal management of power electronics using thermoelectric coolers," in *Proc. 15th Int. Conf. Thermoelectrics*, Pasadena, CA, 1996, pp. 252–255.

[2] H. Böttner, "Micropelt miniaturized thermoelectric devices: Small size, high cooling power densities, short response time," in *Proc. 24th Int. Conf. Thermoelectrics*, Clemson, SC, 2005, pp. 1–8.

[3] G. Min and D. M. Rowe, "Improved model for calculating the coefficient of performance of a Peltier module," *Energy Conv. Manag.*, vol. 41, pp. 163–171, 2000.

[4] H. Böttner, J. Nurnus, A. Gavrikov, G. Kühner, M. Jägle, C. Künzel, D. Eberhard, G. Plescher, A. Schubert, and K.-H. Schlereth, "New thermoelectric components using microsystem technologies," *J. Mircoelectromech. Syst.*, vol. 13.3, pp. 414–420, 2004.

[5] *Ultra-Small Micropelt Peltier Coolers Have 60 Kelvin Delta T for Fiberoptic and Sensor Applications*, Nano Science and Technology Institute [NSTI], 2007, press release [Online]. Available: http://www.nsti.org/press/PRshow.html?id=2249.

[6] A. Rosencwaig, J. Opsal, W. L. Smith, and D. L. Willenborg, "Detection of thermal waves through optical reflectance," *Appl. Phys. Lett.*, vol. 46, pp. 1013–1015, 1985.

[7] G. Tessier, S. Pavageau, B. Charlot, C. Filloy, D. Fournier, B. Cretin, S. Dilhaire, S. Gomes, N. Trannoy, P. Vairac, and S. Voltz, "Quantitative thermoreflectance imaging: Calibration method and validation on a dedicated integrated circuit," *IEEE Trans. Compon. Packag. Technol.*, vol. 30, no. 4, pp. 604–608, Sep. 2007.

[8] D. Lüerßen, J. A. Hudgings, P. M. Mayer, and R. J. Ram, "Nanoscale thermoreflectance with 10 mK temperature resolution using stochastic resonance," in *Proc. 21st SemiTherm*, San Jose, CA, 2005, pp. 253–258.

[9] J. Christofferson and A. Shakouri, "Thermal measurements of active semiconductor micro-structures acquired through the substrate using near IR thermoreflectance," *Microelectron. J.*, vol. 35, pp. 791–796, 2004.

[10] G. Tessier, M. Bardoux, C. Boué, C. Filloy, and D. Fournier, "Back side thermal imaging of integrated circuits at high spatial resolution," *Appl. Phys. Lett.*, vol. 90, pp. 171112-1–171112-3, 2007.

[11] S. Grauby, B. C. Forget, S. Hole, and D. Fournier, "High resolution photothermal imaging of high frequency phenomena using a visible charge coupled device camera associated with a multichannel lock-in scheme," *Rev. Sci. Instrum.*, vol. 70, no. 9, pp. 3603–3608, 1999.

Rajeev Singh received the B.S. and M.S. degrees in electrical engineering from the University of California, Santa Cruz, in 2001 and 2005, respectively. He is currently pursuing the Ph.D. degree in electrical engineering at the University of California, Santa Cruz, working on thin film thermoelectric material and device characterization.

His main interest is in high-speed, low-noise experimentation in the electrical and optical domains.

Joachim Nurnus received the Dr.rer.nat. degree from Albert-Ludwigs Universität Freiburg, Germany, in 2001.

In 1997, he joined the Fraunhofer Society, Fraunhofer-Institut für Physikalische Messtechnik Freiburg, Germany, in the fields of IV–VI- and V–VI-based semiconductors for use in quantum well and superlattices structures. His main work topics were thermoelectric thin-film materials, devices, and measurement techniques in addition to project management. Since 2006, he has been with Micropelt GmbH, Freiburg. As a member of the management team, he is responsible for technology development and project management of customer projects. He has more than 40 publications in conference proceedings, is the author of three chapters in thermoelectrics-related books, and holds several patents.

Zhixi Bian received the B.S. degree in electronics from Nankai University, Tianjin, China, in 1993, the M.S. degree in electronics from Beijing University, Beijing, China, in 1996, and the Ph.D. degree from the University of California, Santa Cruz, in 2004.

He is now a Project Scientist at the University of California, Santa Cruz. His research interests include carrier transport in micro and nano devices, renewable energy, thermoelectric materials, tunable semiconductor lasers, and optoelectronic and photonic integrated circuits.

James Christofferson received the B.S. degree in physics, the M.S. degree in computer engineering, and the Ph.D. degree in electrical engineering from the University of California, Santa Cruz, in 2004.

He is currently a Postdoctoral Researcher in the Quantum Electronics Group, University of California, Santa Cruz.

Ali Shakouri received the B.S. degree from École Nationale Supérieure des Télécommunications de Paris, Paris, France, in 1990 and the Ph.D. degree from the California Institute of Technology, Pasadena, in 1995.

He is a Professor of electrical engineering at the University of California, Santa Cruz. He is the director of the Thermionic Energy Conversion Center, a multi-university research initiative aiming to improve direct thermal-to-electric energy conversion technologies. His current research is on nanoscale heat and current transport in semiconductor devices, submicrometer thermal imaging, microrefrigerators on a chip, and novel optoelectronic integrated circuits.

Dr. Shakouri received the Packard Fellowship in 1999 and the NSF Career Award in 2000.